April 2012
Volume 12
Number 4
pubs.acs.org/crystal

CRYSTAL GROWTH & DESIGN

INTEGRATING THE FIELDS OF CRYSTAL ENGINEERING AND CRYSTAL GROWTH FOR THE SYNTHESIS AND APPLICATIONS OF NEW MATERIALS

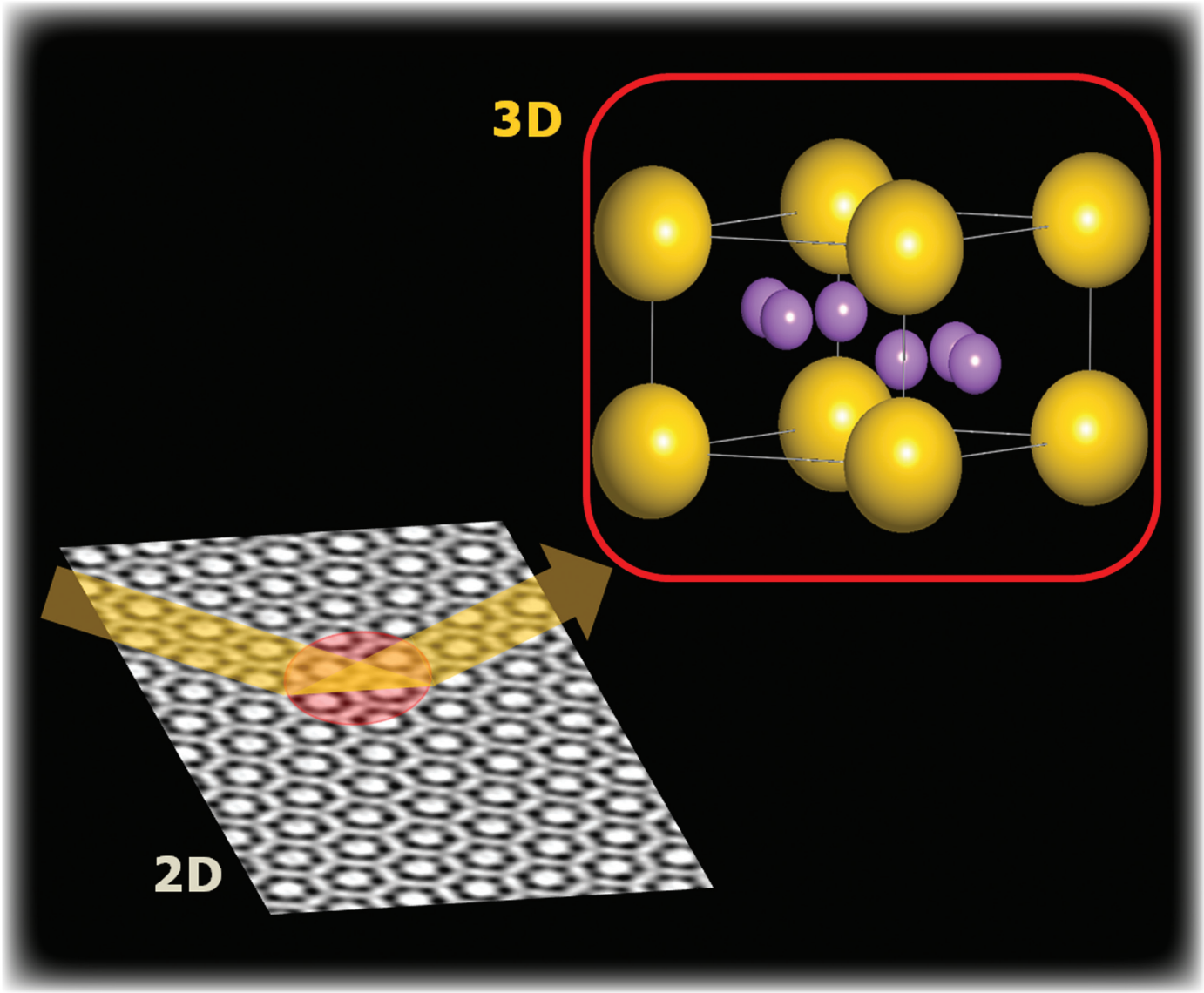

ACS Publications
MOST TRUSTED. MOST CITED. MOST READ.
www.acs.org

CRYSTAL GROWTH & DESIGN

Article

pubs.acs.org/crystal

Meso-Crystallographic Study of a Three-Dimensional Self-Assembled Bimodal Nanocrystal Superlattice

Davide Altamura,[†] Liberato De Caro,[†] Michela Corricelli,[‡,§] Andrea Falqui,[⊥] Marinella Striccoli,[‡,§] M. Lucia Curri,[‡,§] and Cinzia Giannini*[,†]

[†]Istituto di Cristallografia (IC-CNR), via Amendola 122/O, 70126 Bari, Italy

[‡]IPCF-CNR Bari, c/o Department of Chemistry, via Orabona, 4, I-70126 Bari, Italy

[§]Department of Chemistry, University of Bari, via Orabona, 4, I-70126 Bari, Italy

[⊥]Fondazione Istituto Italiano di Tecnologia (IIT), via Morego 30, I-16163 Genova, Italy

Supporting Information

ABSTRACT: Nanocrystal superlattices are attracting significant interest due to novel and peculiar collective properties arising from the interactions of the nanocrystals forming the superlattice. A large variety of superlattice structures can be obtained, involving one or more types of nanocrystals, with different sizes and concentrations. Engineering of the superlattice properties relies on accurate structural and morphological characterization, able to provide not only a fundamental feedback for synthesis procedures, but also relevant insight into their structural properties for possible applications. Electron microscopy and X-ray based techniques are complementary approaches for nanoscale structural imaging, which however become challenging in the presence of building blocks only a few nanometers in size. Here, a structure solution for a three-dimensional (3D) self-assembly of PbS nanocrystals with bimodal size distribution is obtained, by exploiting small-angle X-ray diffraction, transmission electron microscopy, crystallographic procedures, and geometric constraints. In particular, analysis of small-angle X-ray diffraction data, based on the Patterson function and on the single crystal model, is shown to provide relevant information on the 3D superlattice structure as well as on particle size, the scattering signal being sensitive to particles as small as 1.5 nm. The combined approach here proposed is thus demonstrated to effectively overcome important resolution limitations in the imaging of superlattices including small nanocrystals.

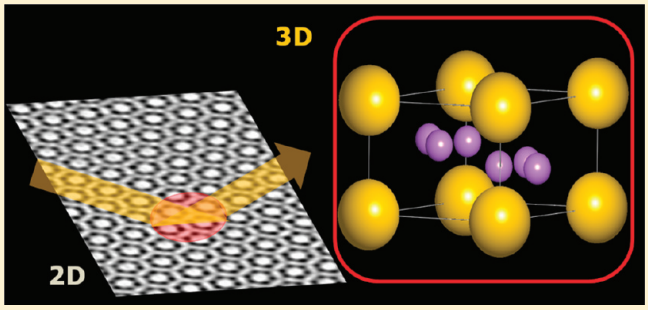

INTRODUCTION

In recent years, significant efforts have been directed toward the preparation of multicomponent superlattices (SLs), either binary (BNSLs)[1−3] or ternary (TNSLs),[4] formed of two or three different types of nanocrystals (NCs) as building blocks of an ordered array, to fabricate innovative materials with enhanced collective properties. The success of such attempts relies on two fundamental conditions. On one hand, the ability to accurately control structural and morphological parameters such as size and shape of the building blocks, which ultimately determine the SL symmetry and structure. On the other hand, the availability of a prompt and reliable feedback on synthesis procedures is crucial, by means of a suitable structural and morphological investigation at each hierarchic level, from the single building block to the entire superlattice. Transmission electron microscopy (TEM) is typically employed, providing two-dimensional (2D) projection images which can be in general not sufficient to derive the three-dimensional (3D) structure of the sample.[5] Electron tomography can be a valuable tool to reconstruct a direct 3D representation of the whole SL structure,[6] although it requires dedicated instrumental equipment and strong constraints on sample characteristics (high stability, transparency to electrons, no organic contamination).[7] However, electron microscopy and tomography need suitable sample preparation and can suffer from insufficient absorption contrast in the case of high organic concentration. This can prevent the imaging of NCs as they are in the assembly, in particular if they are sized only a few nanometers or less, or the image can be misinterpreted in the case of SL complex structures. Even more critical is the high resolution imaging (HRTEM) of single building blocks in the assembly. Moreover the electron beam can cause radiation damage to the organic component of self-assembled SLs.

In this perspective, small and wide-angle X-ray scattering techniques (SAXS, GISAXS, WAXS) have become more and more relevant, since hard X-rays can penetrate deep in the sample, nondestructively probing both morphological and structural properties of the assembly on a large volume.

Received: December 21, 2011
Revised: February 13, 2012
Published: February 22, 2012

ACS Publications © 2012 American Chemical Society

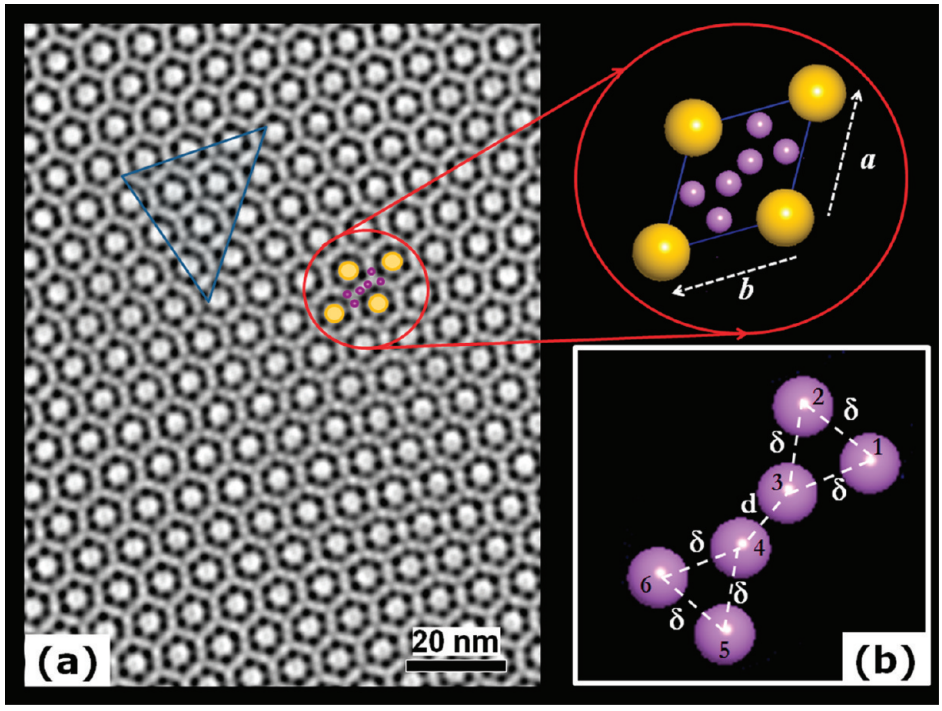

Figure 1. (a) Filtered TEM image of the PbS NC bimodal SL, together with a schematic 2D projection of the unit cell (close-up); (b) scheme of the distances between the small particles in the ideal unit cell.

Neither SAXS, WAXS, nor GISAXS can individually provide a complete morphological and structural characterization, from atomic to mesoscopic length scales; hence they should be synergically exploited. GISAXS[8−10] is especially suitable to simultaneously investigate NC shape and SL structure of assemblies formed on a flat surface. However, even in this case, indexing of 2D diffraction patterns can be in general not sufficient to derive the particle positions in the SL unit cell, and a careful analysis of Bragg diffraction spot intensities would be necessary. This kind of analysis could be in turn not feasible in the case of low intensity of diffraction spots, due for example to the small size of the ordered domains. Moreover, programs for the full analysis of GISAXS patterns from 3D assemblies are still currently under development.[11]

Here, we combine TEM and small-angle X-ray diffraction (SA-XRD), the two most popular and widespread structural characterization techniques, to derive the structure of a 3D self-assembled NCSL, together with morphological details on the building blocks. This study has been performed on a specific bimodal SL obtained by the assembling of PbS NCs with bimodal size distribution, allowing the proposed method to be tested independently of the difference in chemical composition, typically occurring in BNSLs. In particular, the TEM image, suitably filtered, allowed direct observation of the 2D spatial arrangement of the NCs, parallel to the substrate plane. SA-XRD data provided information on the NC positions in the unit cell along the direction normal to the plane of the sample substrate, which, supported by a detailed crystallographic analysis, allowed the NC positions and NC size in both populations forming the superlattice to be determined.

In addition, this 3D crystallographic analysis of the sample structure may provide important feedback in the preparation of bimodal NC superlattices and is expected to be an extremely effective tool adaptable and applicable to more complex geometries and structures, even containing more than two particle types (as for example ternary SLs).

EXPERIMENTAL SECTION

Sample Preparation. PbS NCs with bimodal size distribution were synthesized as explained in the following (see also refs 12 and 17 for details). One millimole of PbO, 2 mL of trioctylphosphine (TOP), and 1.3 mol of oleic acid (OLEA) were added to 20 mL of 1-octadecene (ODE), a noncoordinating solvent, and stirred under vacuum at 120 °C: at this stage the formation of lead-oleate precursors occurred. After about 1 h the bubbling stopped and the solution completely turned to colorless; then the reaction vessel was saturated with N_2: a 20 mM solution of the sulfur precursor, hexamethyldisilathiane (HMDS) in ODE (corresponding to Pb/S molar ratio equal to 50:1) was quickly added and the temperature was cooled down to 80 °C. The growth was carried out at this temperature for 8 min. The synthesis was stopped by removing the heat, and then the solution was allowed to reach room temperature and the NCs were purified using a nonsolvent precipitation procedure, by using a short alkyl chain alcohol (i.e., ethanol). In order to completely remove the excess of OLEA up to three cycles of purification are required. The final precipitate was dried under a nitrogen flow and successively dispersed in toluene.

The bimodal SL was formed by drop casting the toluene solution containing the PbS NCs onto a TEM grid or, alternatively, onto a silicon substrate, and by the subsequent slow solvent evaporation.

XRD Measurements. Small and wide-angle X-ray diffraction data were collected on NC assemblies formed onto silicon substrates. Measurements were performed in coupled sample/detector ($\theta/2\theta$) scan mode (symmetric reflection geometry) by a Bruker D8 Discover, equipped with a Göbel mirror and using Cu Kα radiation. Sample surface was aligned 0.2° off with respect to the specular reflection of the Si substrate, in order to damp the specular reflectivity.

TEM Analysis. TEM micrographs were collected by using a Jeol Jem-1011 microscope, equipped with a W electron source operating at 100 kV voltage and a Gatan SC-1000 Orius Camera.

RESULTS

Transmission Electron Microscopy. Figure 1 shows the filtered TEM image of the assembly of organic capped PbS NCs. This image was obtained from a raw TEM image, similar to that collected on the same sample and reported in a previously published work by the same authors.[12] On the basis of that bare image, the authors inferred the BNSL to be isostructural with $CaCu_5$. On the contrary, the filtering process (see details in the Supporting Information) which led to the image in (Figure 1a) allowed direct observation of the smaller particles and their in-plane arrangement, suggesting an AB_6 stoichiometry of the assembly, differently from the previous hypothesis. The 2D arrangement of the large NCs clearly follows a hexagonal symmetry (see also the Fourier transformed image, Figure S-1 in the Supporting Information).

The measured in-plane lattice parameters, corresponding to the distance between two neighboring big particles, are $a = b = 8.9 \pm 0.3$ nm. Around each large NC, 12 small ones can be readily recognized, defining an AB_6 in-plane stoichiometry of the assembly. The measured diameters of large (A) and small (B) NCs are 3.9 ± 0.4 nm and 1.6 ± 0.2 nm, respectively, where the error bars here reported are representative of the actual size distribution. The 2D projection of the unit cell is schematically represented in the close-up of Figure 1, where NCs are indicated by full circles. Although distortions in distances and angles among B type NCs are clearly visible in the TEM image reported in Figure 1a (see for example the shaded triangular region), such B type NCs can be assumed to be arranged in the ideal unit cell as shown in Figure 1b. In the 2D projection in Figure 1, B type NCs are all distant δ to each other, except the two closest ones in the center (labeled 3 and 4), whose distance has been defined as d. The projected distances δ and d can be related through simple geometrical calculations, by considering the schemes in Figure 1. Because of symmetry, each small NC is at a distance $d/2$ from the edge of the unit cell and is at a distance δ from each of the neighboring two small NCs within the same half unit cell. As a consequence, if d is known, δ can be easily calculated as

$$\frac{\delta}{a} = \cos\left(\frac{\pi}{6}\right)\left[\tan\left(\frac{\pi}{6}\right) - \frac{d}{a}\right] \quad (1)$$

where a is the lattice parameter. The distance d, along the longest diagonal in the unit cell ($b-a$), is the smallest (in-plane) projected distance between the B type particles, which is equal to 2.1 ± 0.1 nm; the other in-plane distances can be assumed approximately constant and equal to $\delta = 2.6 \pm 0.3$ nm.

Small Angle X-ray Diffraction. In Figure 2a the experimental (dotted line) and simulated (solid line) SA-XRD patterns are reported as a function of the scattering angle 2θ (bottom axis) and the scattering vector length $Q = 2 \sin \theta/\lambda$ (top axis). A constant background (equal to the smallest intensity value in the pattern) was interpolated and subtracted from the experimental data in order to enhance the visibility of the diffraction peaks. Equally spaced peaks, up to the 10th order, are clearly visible and have been marked by the (00l) Miller indices. The (00l) reflections are related to the repeat distance (period) c of the structure perpendicularly to sample surface (defined as the z axis), which can be estimated as $c = 1/\Delta Q$, where ΔQ is the difference in Q units between consecutive intensity maxima. A repeat distance of $c = 6.4 \pm 0.1$ nm has been directly derived from the ΔQ spacing in the experimental curve and defined as the c lattice parameter.

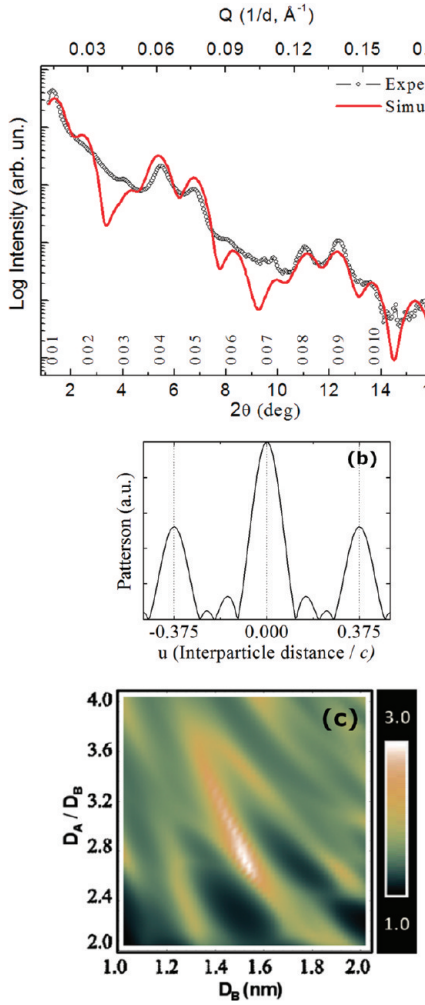

Figure 2. (a) Experimental (symbols) and simulated (solid line) small angle XRD patterns of the BSD sample; (b) Patterson function calculated from the experimental data in panel (a); (c) 2D plot of the FOM for the fit in panel (a), as a function of particle size.

The absence of other (hkl) reflections allows a one-dimensional (1D) approach in X-ray data analysis. Particles arrangement along z was obtained by calculating the 1D Patterson function as the inverse Fourier transform of the SA-XRD pattern, which is reported in Figure 2b, and the successive simulation of the SA-XRD data (Figure 2a). The peaks in the Patterson function $P(\boldsymbol{u})$ (see Supporting Information) generally represent "interatomic" distances in units of c (in this case interparticle distances), along the z-axis in the SL unit cell. In the general 3D case, the Patterson function depends on the "interatomic" vectors $\boldsymbol{u}$, while here it is applied to the 1D case along the z axis, so that it only depends on the z coordinate, and the scalar quantity u is used here to define interparticle distances along the z axis. The Patterson function being centrosymmetric by definition, only half of the peaks are meaningful. An interparticle distance $u_1 = 0.375$ can be derived from Figure 2b, which can be associated with the distance along z of the B type particles from the A type NC within the unit cell. Patterson peak intensity is indeed proportional to the scattering power of the particles (hence it increases with particle volume) separated by the generic vector $\boldsymbol{u}$; therefore an A type NC particle will certainly contribute to the only peak visible in Figure 2b (at u_1). Also, the value of the c parameter

prevents two or more A type particles being placed one on top of the other along z, within the unit cell. Therefore, once the origin in the unit cell is chosen at the A type NC position (z = 0), u_1 denotes the distance, in units of c, of one or more B type NCs from the A type one. As a consequence, the B type NCs can be expected on two layers equally distant ($\pm u_1$) from the A type NC, with z coordinates $z_1 = u_1$ and $z_2 = 1 - z_1$. The as-derived z coordinates have been used as a starting point for the SA-XRD pattern simulation, which has been performed according to a simple single crystal model in which the "atomic" positions are occupied by the NCs. The NC scattering (or form) factor has been calculated as the Fourier transform of the NC shape function $S(\boldsymbol{Q})$ (see Supporting Information, Eq. s2.b), which is equal to 1 within the particle volume and 0 outside. This corresponds to the assumption of a constant electron density distribution in the volume of each single NC. The assumption of an equal electron density for A and B type particles is justified by the wide angle XRD pattern (see Figure S-2 in the Supporting Information), featuring the only rock salt (CsCl type) crystalline phase of PbS. Moreover, a spherical shape has been assumed for the NCs, also based on the TEM data. The X-ray intensity scattered by the SL has been then calculated for the (00l) reflections as a function of Q, as usual in crystallography (see Supporting Information).

Although NCs should be in general considered as core−shell particles, the shell being formed by organic ligands, the scattering contribution of the last, in the SA-XRD, has been neglected, because of its significantly lower scattering power with respect to Pb and S.

The independent parameters in the simulation are NC diameters for the two populations, z_1, and the number of B type particles at z_1 and z_2.

Deeper minima in the simulated patterns resulted with respect to the experimental one (see Figure 2a). Such evidence can be ascribed to the particle finite size distribution, which is inherent in the real sample and leads to a damping of intensity oscillations in the experimental pattern and possibly to additional structured background due to off-specular X-ray reflectivity from substrate regions not fully covered by NCs.

A figure of merit (FOM), expressing the goodness of the fit, has been considered, defined as the inverse of the reconstruction error, that is, FOM = 1/R, where

$$R = \frac{\sum |\sqrt{I_{sim}} - \sqrt{I_{exp}}|}{\sum \sqrt{I_{exp}}} \qquad (2)$$

where I_{sim} and I_{exp} are the simulated and the measured intensities, respectively, at each point.

The largest obtained FOM value (approximately 3) corresponds to the smallest value of the reconstruction error ($R \cong 0.33$), which led to a good matching between experimental (dotted line) and simulated (solid line) patterns (Figure 2a). Such best fit corresponds to the following assumptions. The B type particles are equally distributed on two layers in the unit cell — being reasonably based on symmetry considerations — at $z_1 = 0.385 \pm 0.010$ and $z_2 = 0.615 \pm 0.010$ (in agreement with the Patterson function in Figure 2b), and the NC diameter values are $D_A = 4.0 \pm 0.3$ nm and $D_B = 1.5 \pm 0.1$ nm, for the A and B type particles, respectively (in good agreement with the TEM observations). The estimated number of unit cells stacked perpendicularly to the substrate is 5. It should be noted that the error bars on the NC sizes reported above derive from the fit of the SA-XRD, and are therefore related to the error in determining the average values of NC diameters for the two populations, each assumed monodisperse in size.

The FOM has been reported in Figure 2c as a function of D_B and the ratio D_A/D_B. The values indicated by the color scale are such that the higher the value the better the agreement between simulation and experiment. A FOM value equal to 1 indicates therefore a complete disagreement.

Again, the distance between the two layers of B type particles, which is equal to $(z_2 - z_1)c = 1.5$ nm, prevents two B type particles from being located one on the top of the other, since they would be in contact. This, together with the 2D projection image of Figure 1a, implies that there cannot be less nor more than six small particles in the unit cell, so that the "volume stoichiometry" of the 3D SL is actually AB_6, and there are three B type particles on each layer (at z_1 and z_2).

DISCUSSION

The SL structure can be completely defined once all coordinates of each particle in the unit cell are known. The SL unit cell parameters, and the NCs in-plane (x, y) and out-of-plane (z) coordinates, have been derived from TEM and SA-XRD data, respectively. The in-plane coordinates of the B type NCs (as represented in the ideal structure of Figure 1b) can be expressed as a function of the d/a ratio (equal to 0.24 ± 0.02), between the distance d and the unit cell parameter a (see Supporting Information). It remains to define which B type particles the z_1 and z_2 coordinates are associated with. As a first constraint, the two B type particles 3 and 4 in Figure 1b should have different z coordinates. This is based on symmetry considerations (there must be three particles at z_1 and z_2), and especially on the fact that in this case the free space to accommodate the ligand molecule between the particles would

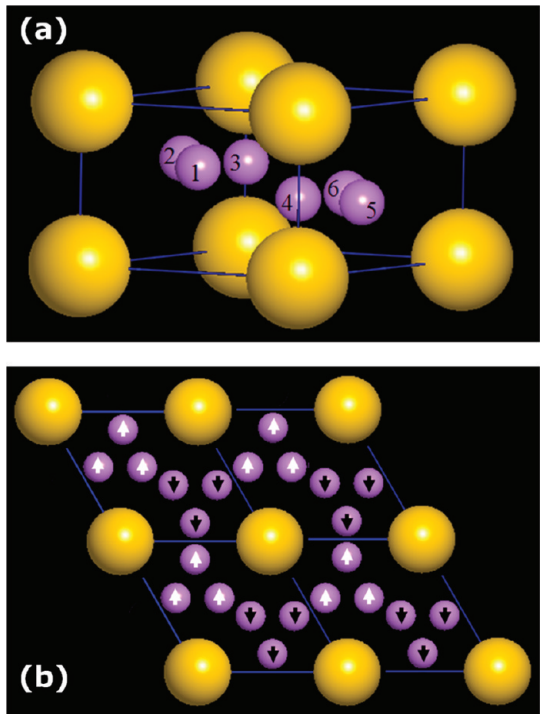

Figure 3. Diagram of the 3D structure solution proposed for the bimodal SL: (a) unit cell; (b) four unit cells, seen in the (001) projection.

dx.doi.org/10.1021/cg201682s | Cryst. Growth Des. 2012, 12, 1970−1976

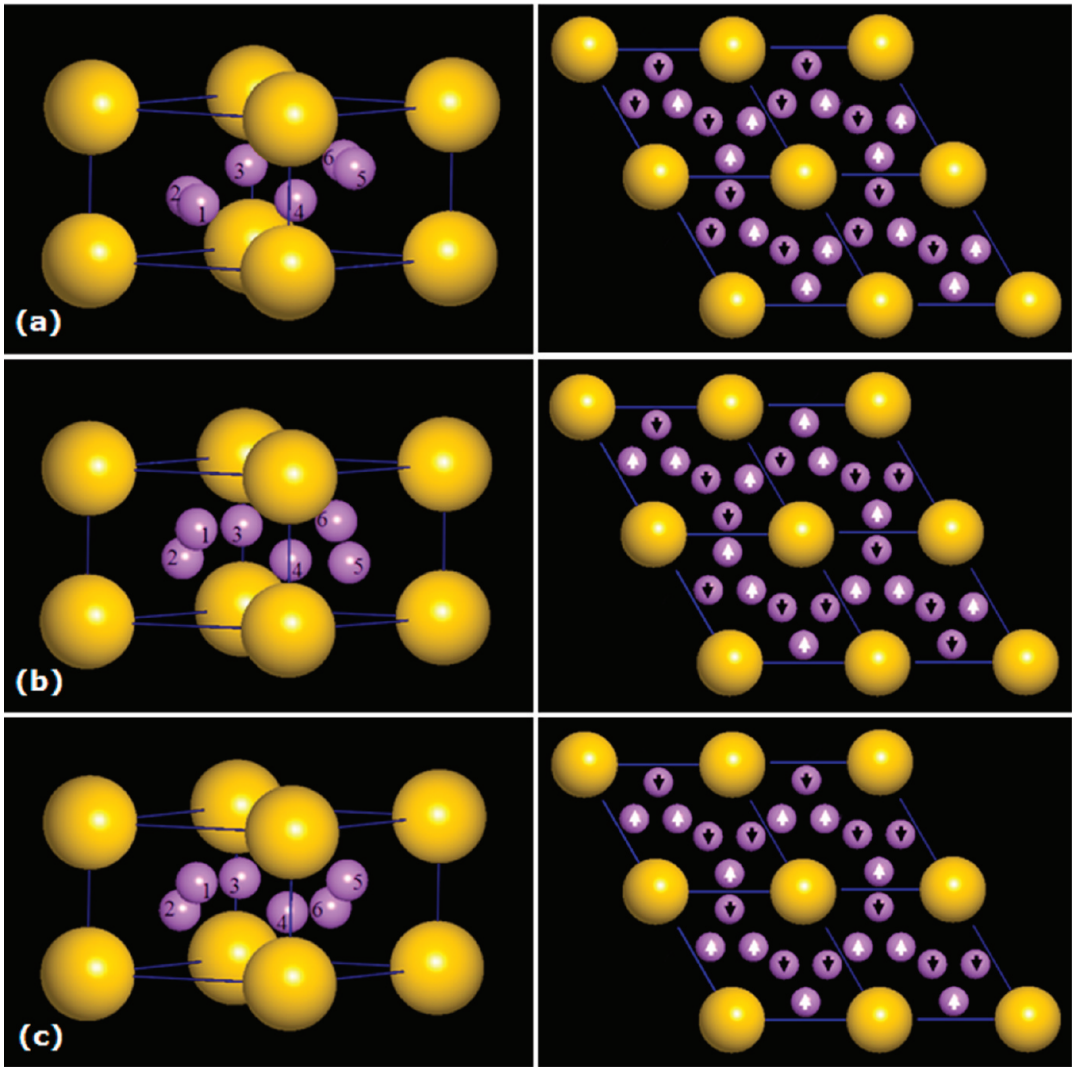

Figure 4. Diagrams of alternative structure models (perspective view) obtained from different combinations of the z coordinates of the small particles: particles 1, 2 and 5, 6 on the same layer (a), and on different layers (b, c).

be 1.1 nm, whereas only 0.6 nm would be available for the ligand if the two particles lie on the same plane (same z value). Such distance in principle would not be enough to accommodate the ligand shell. In fact, the full extended length of OLEA is 1.8 nm[13] and, although shorter interparticle distances can be justified by molecules interdigitation and/or by compression of the ligand shells of neighboring NCs, the lower value reported so far is 0.8 nm, and shorter distances are very unlikely to occur.[14,15]

The constraint for particles 3 and 4, together with that on the number of particles (three) in each layer, lead to only a few possible cell structures (see Figure 3, and Figure 4), thus suggesting that translational periodicity should occur also in the z coordinates of the B type particles, ultimately leading to a 3D SL. In order to derive the actual SL unit cell structure, the symmetry properties of the unit cells reported in Figure 3 and Figure 4, were studied by calculating a X-ray powder diffraction pattern and looking for a structure solution by using the EXPO2009 crystallographic program.[16] The only structure solution returned by the program is the one reported in Figure 3, which is compatible with $P321$ and $P\bar{3}$ space group symmetries.

The SL structure could be thus expected to consist of one or more domains each characterized by one of the possible unit cell types. However, there are three main arguments supporting the model of Figure 3 as the most favored one. First, the models of the type in Figure 3, and Figure 4a should indeed be favored based on symmetry considerations; moreover, these are the only models mutually compatible, whereas the transition between any other combination of cell types would imply the particles labeled 3 and 4 to lie on the same plane, leading to distortions in distances and/or angles. The systematic occurrence of such transitions is unlikely, as testified by the large ordered areas revealed by TEM analysis. As a consequence, a well-defined structure model for the assembly should occur with a higher probability, leading to an actual 3D bimodal SL.

The repetition of the unit cell of Figure 3a is schematically represented in Figure 3b, in the (001) projection. The B type particles having z_1 or z_2 coordinates are labeled by arrows pointing down (black) or up (white), respectively. The same labeling has been used in Figure 4. It should be noted that the unit cells represented in Figure 4a,c could fill the entire space preserving translational periodicity, with in plane period equal to a, whereas the periodic repetition of the "unit cell" in Figure

4b would violate the constraint on particles 3 and 4. In this case, a lattice could still be constructed by systematically alternating a cell with its enantiomorphous (given by the specular image of the cell with respect to a plane parallel to the longest diagonal of the cell, that is, $b-a$, and to the c axis), in which case a SL with in plane period equal to $2a$ would result.

Finally, the model of Figure 3 is the only one where a unique constant distance (of 2.6 nm center-to-center) results between each pair of B type particles. The center-to-center distance between an A type and a neighboring B type particle would be 5.6 nm in any case, so that the edge to edge distance is 2.5 nm. Therefore, the overall results and considerations here reported indicate that the most probable 3D SL description is given by the periodic repetition of the unit cell represented in Figure 3a.

CONCLUSIONS

This study provides a structure solution for a bimodal 3D self-assembly of PbS NCs, by exploiting SA-XRD data from a typical laboratory equipment, combined with TEM experiments, and crystallographic procedures. Geometric considerations were used as constraints in deriving the structure solution. In particular, the analysis of SA-XRD data, based on the Patterson function, is shown to provide relevant information on the SL structure as well as on particle size, the scattering signal being particularly sensitive to very small particle size (below 2 nm). The presented meso-crystallographic approach is demonstrated as a powerful tool to investigate the structure of NCSLs and could significantly contribute in answering the highly demanding questions of structural studies on nano-metamaterials at different length scales. Moreover, it could be possibly extended to higher complexity structures, even containing a larger variety of building blocks, and contribute in elucidating the mechanisms of NC superlattice formation and in SL engineering. It can be applied to many different nanoparticle 3D assemblies, the crystallinity of the SL building blocks not being a specific requirement both for TEM and SA-XRD analyses. By exploiting the X-ray high penetration depth and the large sampled volumes, a representative 3D imaging of large and thick assemblies can indeed be achieved, even in the presence of a large fraction of organic material that could hinder the successful use of electron tomography based approaches.

ASSOCIATED CONTENT

Supporting Information

Supporting Information (details on the TEM image filtering process, the Patterson function used for the small angle XRD data analysis, the wide angle XRD data and relevant Rietveld analysis, the theoretical and mathematical aspects of the small angle XRD data simulation, the determination of the SL structure) is available free of charge via the Internet at http://pubs.acs.org.

AUTHOR INFORMATION

Corresponding Author

*E-mail: cinzia.giannini@ic.cnr.it. Phone: 0039-080-592-9167. Fax: 0039-080-592-9170.

Notes

The authors declare no competing financial interest.

ACKNOWLEDGMENTS

This work has been partially supported by the SEED project "X-ray synchrotron class rotating anode microsource for the structural micro imaging of nanomaterials and engineered biotissues (XMI-LAB)"- Italian Institute of Technology (IIT) Protocol No. 21537 of 23/12/2009 and by the EU FP7 project "METACHEM" (Grant Agreement CP-FP 228762-2). Mr. R. Lassandro is acknowledged for his full technical support in the XRD laboratory.

REFERENCES

(1) Dong, A. G.; Chen, J.; Vora, P. M.; Kikkawa, J. M.; Murray, C. B. Binary nanocrystal superlattice membranes self-assembled at the liquid–air interface. *Nature* **2010**, *466*, 474–477.

(2) Ye, X.; Chen, J.; Murray, C. B. Polymorphism in self-assembled AB6 binary nanocrystal superlattices. *J. Am. Chem. Soc.* **2011**, *133*, 2613–2620.

(3) Chen, Z.; O'Brien, S. Structure direction of II-VI semiconductor quantum dot binary nanoparticle superlattices by tuning radius ratio. *ACS Nano* **2008**, *2*, 1219–1229.

(4) Evers, W. H.; Friedrich, H.; Filion, L.; Dijkstra, M.; Vanmaekelbergh, D. Observation of a ternary nanocrystal superlattice and its structural characterization by electron tomography. *Angew. Chem., Int. Ed.* **2009**, *48*, 9655–9657.

(5) Evers, W. H.; De Nijs, B.; Filion, L. C.; Castillo, S. I. R.; Dijkstra, M.; Vanmaekelbergh, D. A. M. Entropy-driven formation of binary semiconductor-nanocrystal superlattices. *Nano Lett.* **2010**, *10*, 4235–4241.

(6) Friedrich, H; Gommes, C. J.; Overgaag, K.; Meeldijk, J. D.; Evers, W. H.; De Nijs, B.; Boneschanscher, M. P.; De Jongh, P. E.; Verkleij, A. J.; De Jong, K. P.; et al. Quantitative structural analysis of binary nanocrystal superlattices by electron tomography. *Nano Lett.* **2009**, *9*, 2719–2724.

(7) Midgley, P. A.; Dunin-Borkowski, R. E. Electron tomography and holography in materials science. *Nat. Mater.* **2009**, *8*, 271–280.

(8) Renaud, G.; Lazzari, R.; Leroy, F. Probing surface and interface morphology with grazing incidence small angle X-ray scattering. *Surf. Sci. Rep.* **2009**, *64*, 255–380.

(9) Choi, J. J.; Bealing, C. R.; Bian, K.; Hughes, K. J.; Zhang, W.; Smilgies, D.-M.; Hennig, R. G.; Engstrom, J. R.; Hanrath, T. Controlling nanocrystal superlattice symmetry and shape-anisotropic interactions through variable ligand surface coverage. *J. Am. Chem. Soc.* **2011**, *133*, 3131–3138.

(10) Bian, K.; Choi, J. J.; Kaushik, A.; Clancy, P.; Smilgies, D.-M.; Hanrath, T. Shape-anisotropy driven symmetry transformations in nanocrystal superlattice polymorphs. *ACS Nano* **2011**, *5*, 2815–2823.

(11) Buljan, M.; Radic, N.; Bernstorff, S.; Drazic, G.; Bogdanovic-Radovic, I.; Holy, V. Grazing-incidence small-angle X-ray scattering: application to the study of quantum dot lattices. *Acta Crystallogr.* **2012**, *A68*, 124–138.

(12) Corricelli, M.; Altamura, D.; De Caro, L.; Guagliardi, A.; Falqui, A.; Genovese, A.; Agostiano, A.; Giannini, C.; Striccoli, M.; Curri, M. L. Self-organization of mono- and bi-modal PbS nanocrystal populations in superlattices. *CrystEngComm* **2011**, *13*, 3988–3997.

(13) Bodnarchuk, M. I.; Kovalenko, M. V.; Heiss, W.; Talapin, D. V. Energetic and entropic contribution to self-assembly of binary nanocrystal superlattice: temperature as the structure-directing factor. *J. Am. Chem. Soc.* **2010**, *132*, 11967–11977.

(14) Dong, A.; Ye, X.; Chen, J.; Murray, C. B. Two-dimensional binary and ternary nanocrystal superlattices: the case of monolayers and bilayers. *Nano Lett.* **2011**, *11*, 1804–1809.

(15) Lee, B.; Podsiadlo, P.; Rupich, S.; Talapin, D. V.; Rajh, T.; Shevchenko., E. V. Comparison of structural behavior of nanocrystals in randomly packed films and long-range ordered superlattices by time-resolved small angle X-ray scattering. *J. Am. Chem. Soc.* **2009**, *131*, 16386–16388.

(16) Altomare, A.; Camalli, M.; Cuocci, C.; Giacovazzo, C.; Moliterni, A.; Rizzi, R. EXPO2009: structure solution by powder data in direct and reciprocal space. *J. Appl. Crystallogr.* **2009**, *42*, 1197−1202.
(17) Altamura, D.; Corricelli, M.; De Caro, L.; Guagliardi, A.; Falqui, A.; Genovese, A.; Nikulin, A. Y.; Curri, M. L.; Striccoli, M.; Giannini, C. Structural investigation of three-dimensional self-assembled PbS binary superlattices. *Cryst. Growth Des.* **2010**, *10*, 3770−3774.

SUPPORTING INFORMATION

for

Meso-Crystallographic study of a Three-Dimensional Self-assembled Bimodal Nanocrystal Superlattice

Davide Altamura[1], Liberato De Caro[1], Michela Corricelli[2,3], Andrea Falqui[4], Marinella Striccoli[2,3], M. Lucia Curri[2,3], and Cinzia Giannini[1]*

[1]Istituto di Cristallografia (IC-CNR), via Amendola 122/O, 70126 Bari, Italy; [2]IPCF-CNR Bari, c/o Department of Chemistry, Via Orabona, 4, I-70126 Bari, Italy; [3]Department of Chemistry University of Bari, Via Orabona, 4, I-70126 Bari, Italy; [4]Fondazione Istituto Italiano di Tecnologia (IIT), via Morego 30, 16163 Genova, Italy.

TEM ANALYSIS

In Fig. S-1 are reported the as-collected TEM image, Fig. S-1(a), and the corresponding zoomed image, Fig. S-1(b). The small nanocrystals (NCs) cannot be distinguished, and they can be supposed to form the quasi-continuous layers among the big particles. A filtering process has been therefore applied to Fig. S-1(b); the contrast in the TEM image was reversed, and its 2D Fourier Transform (FT) calculated. The FT modulus was then filtered by cutting all the intensity below a suitable threshold, leading to a better visibility of the spots. By calculating the inverse FT, the image reported in Fig. 1(a) (main text) was obtained, which allowed to clearly visualize the smaller NCs as well. The filtering process, by selecting mainly the diffracted intensity close to the Bragg spots, allowed to suppress almost all the noise and defect contributions in the original image. As a consequence, the structural order in Fig. 1(a) is enhanced with respect to the actual structure.

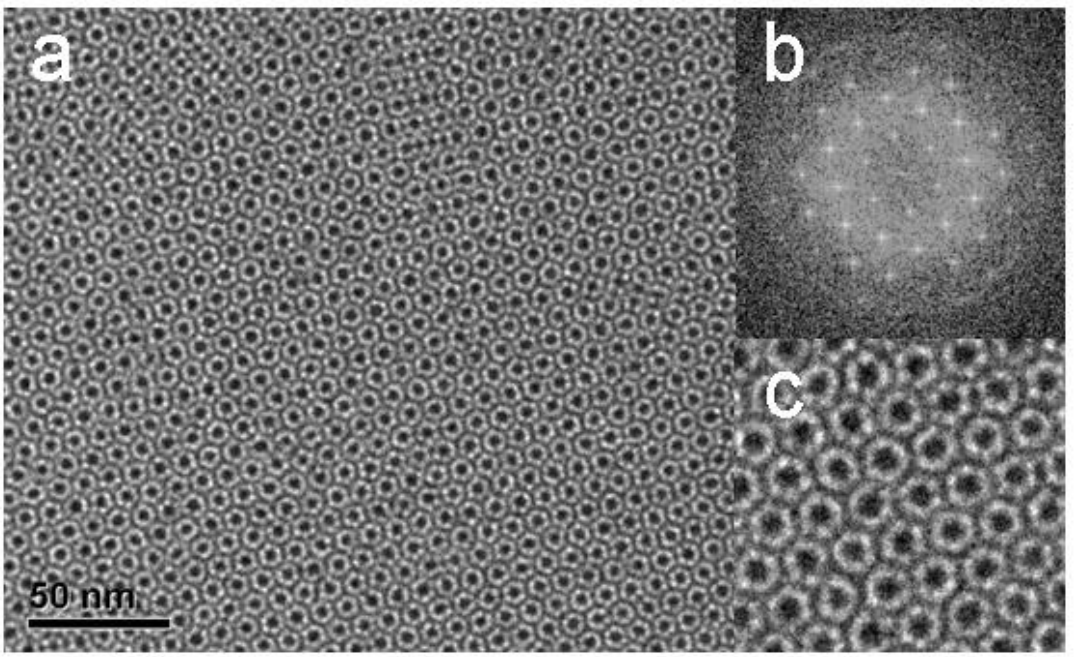

Fig. S-1 TEM analysis of the PbS bimodal SL: unfiltered large field of view (a), Fourier transform (b), and zoomed image (c).

.

PATTERSON FUNCTION

The Patterson function P(***u***) is the convolution of the electron density ρ(***r***) with ρ (-***r***). P(***u***) can be directly obtained from the experimental data as the inverse Fourier transform of the measured scattered intensity. In the traditional case of a crystal, P(***u***) can be calculated as a Fourier series with coefficients given by the structure factors moduli $|F_{\boldsymbol{h}}|$ (where the vector ***h*** has components *h*,*k*,*l*), that are proportional to the measured X-ray diffraction peak intensities [1,2]:

$$P(\boldsymbol{u}) = \frac{1}{V}\sum_{\boldsymbol{h}} |F_{\boldsymbol{h}}|^2 \cos(2\pi \boldsymbol{h}\cdot\boldsymbol{u}) \qquad \text{(s1)}$$

where $\boldsymbol{h}$ is the scattering vector associated with the particular reflection (*hkl*), $\boldsymbol{u}$ a real space vector, and V the volume of the unit cell. The Patterson function is therefore always centrosymmetric. The P($\boldsymbol{u}$) peaks correspond to all possible interatomic vectors $\boldsymbol{u}$ within the unit cell, being the height of each peak proportional to the atomic numbers of the atoms connected by the vector $\boldsymbol{u}$, and to the multiplicity of the same vector. Given N atoms in the unit cell, N_2 peaks are always expected in the Patterson map, N^2 of which (corresponding to the zero distance of each atom with itself) are superimposed into the origin. In order to obtain sharper peaks in the Patterson function, the coefficients $|F_{\boldsymbol{h}}(E_{\boldsymbol{h}}\text{-}1)|^2$ were used in (Eq. s1) for the calculation, instead of $|F_{\boldsymbol{h}}|^2$, as in conventional crystallography, where $E_{\boldsymbol{h}}$ are the normalized structure factors [1] and the term (-1) serves to damp the peak in the origin and make the others more visible [2].

WIDE ANGLE XRD

The fit was performed by FullProf [3], taking into account the instrumental profile, and assuming a single population of PbS NCs with isotropic shape, Fig. S-2(a). The fit returned an average particle diameter of 2.8 nm (for spherical shape), which is significantly different from NC size in both populations (average diameters 3.9 and 1.5 nm respectively, as derived by TEM) and is therefore certainly affected by both size contributions. The WA-XRD pattern can be indeed fitted also by assuming two monodisperse PbS NC populations with the expected particle diameters, as it can be seen in Fig. S-2(b). The PbS rock salt crystalline phase is thus confirmed for both NC populations.

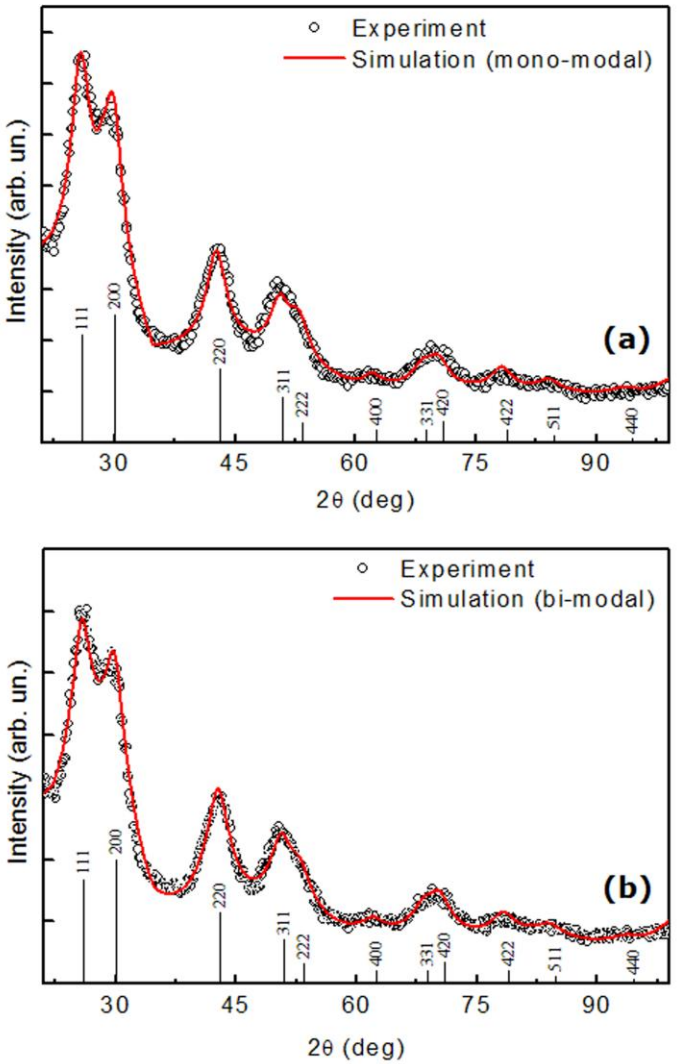

Figure S-2 WA-XRD experimental pattern (symbols) and fit (line) performed for mono-modal (a) and bi-modal (b) size populations (with 3.9 and 1.5 nm NP diameters); expected reflections for the PbS rock salt cubic phase are also reported**.**

SIMULATION OF THE SA-XRD PATTERN

The diffracted intensity I(Q) was calculated as the product of the square modulus of the unit cell structure factor F(Q) times the square modulus of the 1D interference function (due to lattice periodicity) S(Q) [1], expressed by

$$\mathrm{F}(Q) = f_{\mathrm{A}} + f_{\mathrm{B}}\left[\mathrm{n}_1\exp\left(2\pi\mathrm{i}Q\mathrm{z}_1 c\right) + \mathrm{n}_2\exp\left(2\pi\mathrm{i}Q\mathrm{z}_2 c\right)\right] \tag{s2.a}$$

$$S(Q) = \sum_{N=0}^{m}\exp\left(2\pi\mathrm{i}Q\mathrm{N}c\right) \tag{s2.b}$$

where m is the number of SL unit cells stacked along the normal to sample surface, n_1 and n_2 are the number of small particles having components of the position vector z_1 and z_2, respectively, along the surface normal, and the big/small particle scattering factors f_A / f_B have been assumed to be the spherical form factors [1,4]

$$f(Q) = \int_0^R 4\pi r^2 \frac{\sin\left(2\pi rQ\right)}{2\pi rQ}dr = \frac{-2\pi RQ\cos\left(2\pi RQ\right) + \sin\left(2\pi RQ\right)}{2\pi^2 Q^3} \tag{s3}$$

being R the particle radius.

DETERMINATION OF THE SL STRUCTURE

Calculation of in-plane particle coordinates

Components along the basis vectors ***a*** and ***b***, as a function of the ratio $d_f = d/a$, based on the scheme of Fig. 1(b) in the main text

$$x_1 = \frac{1}{2}\left[1 + \frac{d_f}{2\cos\left(\pi/6\right)}\right] \qquad y_1 = \frac{d_f}{2\cos\left(\pi/6\right)}$$

$$x_2 = 1 - \frac{d_f}{2\cos\left(\pi/6\right)} \qquad y_2 = \frac{1}{2}\left[1 - \frac{d_f}{2\cos\left(\pi/6\right)}\right] \tag{s4}$$

$$x_3 = \frac{1}{2}\left[1 + \frac{d_f}{2\cos\left(\pi/6\right)}\right] \qquad y_3 = \frac{1}{2}\left[1 - \frac{d_f}{2\cos\left(\pi/6\right)}\right]$$

The other three particles (labeled 4,5,6) located in the second half of the unit cell have the ***a*** and ***b*** components respectively interchanged.

Parameters used for the calculation of the powder diffraction pattern

- Lattice parameters : $a = b = 8.9$ nm , $c = 6.4$ nm, $\alpha = \beta = 90°$, $\gamma = 120°$

- Nanoparticle in plane coordinates from Eq. 2s; out of plane (z) coordinates are : $z_1 = 0.385$ and $z_2 = 1 - 0.385 = 0.615$.

References

(S1) Giacovazzo, C. et al. *Fundamentals Of Crystallography*, Oxford University Press, New York, 1995; pp 144–147, 150–152, 321–328.

(S2) Giacovazzo, C. *Direct Phasing in Crystallography -Fundamentals and Applications*, Oxford University Press, Inc., New York 1998; pp 183–186.

(S3) http://www-llb.cea.fr/fullweb/

(S4) Renaud, G.; Lazzari, R.; Leroy, F. *Probing surface and interface morphology with Grazing Incidence Small Angle X-Ray Scattering*. Surf. Sci. Reports 2009, 64, 255–380.